

1 Combining Visual Cues with Interactions
2 for 3D-2D Registration in Liver Laparoscopy

3 Yamid Espinel,¹ Erol Özgür,¹ Lilian Calvet,^{1,2}

Bertrand Le Roy,^{1,3} Emmanuel Buc,^{1,2} Adrien Bartoli¹

4 **affiliations:** ¹EnCoV, Institut Pascal, UMR 6602 CNRS/Université Clermont-Auvergne,
5 Clermont-Ferrand, France

6 ²University Hospital of Clermont-Ferrand, France

7 ³University Hospital of Saint-Étienne, France

8 **abbreviated title:** 3D-2D Registration in Liver Laparoscopy

9 **correspondence:** Faculté de Médecine, Batiment 3C, 28 place Henri Dunant, 63001 Clermont-
10 Ferrand, France. e-mail: yamid.espinel_lopez@uca.fr

11 **Abstract**

12 Augmented Reality (AR) in monocular liver laparoscopy requires one to register a
13 preoperative 3D liver model to a laparoscopy image. This is a difficult problem because
14 the preoperative shape may significantly differ from the unknown intraoperative shape
15 and the liver is only partially visible in the laparoscopy image. Previous approaches are
16 either manual, using a rigid model, or automatic, using visual cues and a biomechanical
17 model. We propose a new approach called the hybrid approach combining the best of
18 both worlds. The visual cues allow us to capture the machine perception while user
19 interaction allows us to take advantage of the surgeon’s prior knowledge and spatial un-
20 derstanding of the patient anatomy. The registration accuracy and repeatability were
21 evaluated on phantom, animal ex-vivo and patient data respectively. The proposed
22 registration outperforms the state of the art methods both in terms of accuracy and
23 repeatability. An average registration error below the 1 cm oncologic margin advised
24 in the literature for tumour resection in laparoscopy hepatectomy was obtained.

25 **keywords:** Laparoscopy, liver, registration, 3D-2D, augmented reality

1 Introduction

One of the main current limitations of laparoscopy is the difficulty to accurately localize the target organ’s internal anatomy, owing to the absence of tactile feedback. This is a particularly important issue for the liver, which may contain malignant tumours to be precisely resected with an oncologic margin. Augmented Reality (AR) is a promising approach to overcome this limitation. The key idea is to overlay information extracted from a preoperative CT volume onto the laparoscopy images. These information may be the tumours and their oncologic margin but also the vascular structure. During the initial exploration phase of a surgery, AR allows the surgeon to perform resection planning. An example of augmented laparoscopic image is shown in Figure 1. The laparoscopic image is overlaid with the projection onto the liver surface of the tumour’s boundary which is invisible to the laparoscope, along with a planned resection path following the oncologic margin. Compared to classical mental mapping approaches used in laparoscopy such as [1], AR systems like the proposed one cope with the deformation undergone by the liver from the preoperative to the intraoperative stages. Also, by directly overlaying the laparoscopic images with the registered preoperative model of the intraparenchymal structures, rather than mentally mapping them from a separate screen to the laparoscopic image, surgeons can be more confident regarding the real location of these structures.

A typical AR-based guidance system for laparoscopy is composed of two stages: *(i)* an initial registration stage during which the preoperative 3D model is aligned, or *registered*, to intraoperative laparoscopic images; *(ii)* an update stage during which the model is automatically registered to a new laparoscopic image by tracking visual cues. Current systems handle limited smooth changes at best, such as those induced by breathing, heart beating and manipulations with surgical instruments, but fail with irregular changes such as cutting or tearing. In this work we focus on the initial smooth deformable registration stage *(i)* which is a very challenging and currently highly researched problem. Its principle is illustrated in Figure 2.

The difficulty of the registration problem is two-fold. First, the liver is only partially

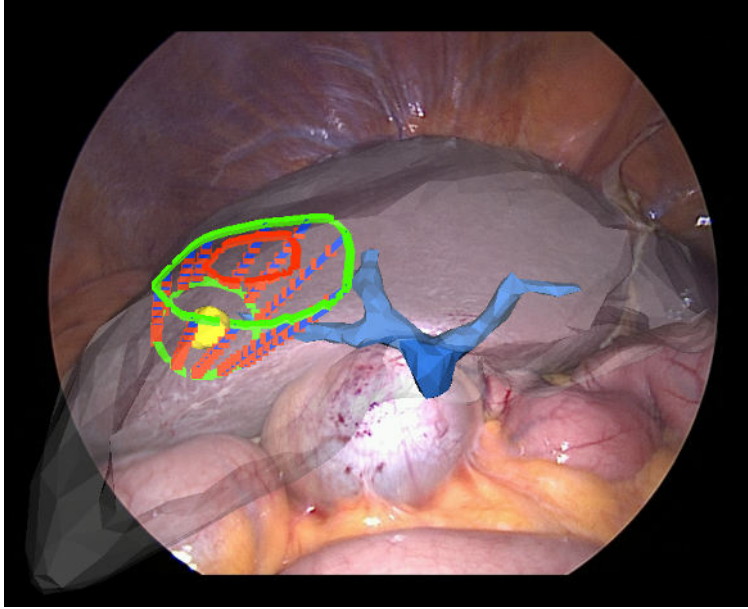


Figure 1: Example of AR used to overlay a laparoscopic image with the projection of a tumour’s boundary (in red) with its oncologic margin (in green) onto the liver’s surface, as produced by our system. The subsurface tumour (in yellow) and major vessels (in blue) are also made visible. The planned resection path is marked in blue. Red dots are placed at every centimeter from the liver surface to the tumour. The resection mark follows the 1 centimeter oncologic margin advised in the literature for the treatment of colorectal cancer liver metastasis (CRLM) and hepatocellular carcinoma (HCC).

54 visible in the laparoscopy image due to its large size and proximity to the laparoscope.
55 Second, the liver deforms substantially between the preoperative volume and the laparo-
56 scopy image due to the pneumoperitoneum (the intraoperative CO₂ gas insufflation) and its
57 manipulation by the surgical instruments. We focus on regular laparoscopy, which in terms
58 of computer vision is a single monocular pin-hole camera, and forms the standard in oper-
59 ating theatres. It is obvious that any system designed for monocular laparoscopy extends to
60 stereo-laparoscopy.

61 Currently, the most promising registration approaches share two main features. First,
62 they solve the registration from the image contents only, without resorting to external hard-
63 ware. Second, they use a *preoperative 3D model* consisting of the liver, tumours and vessels

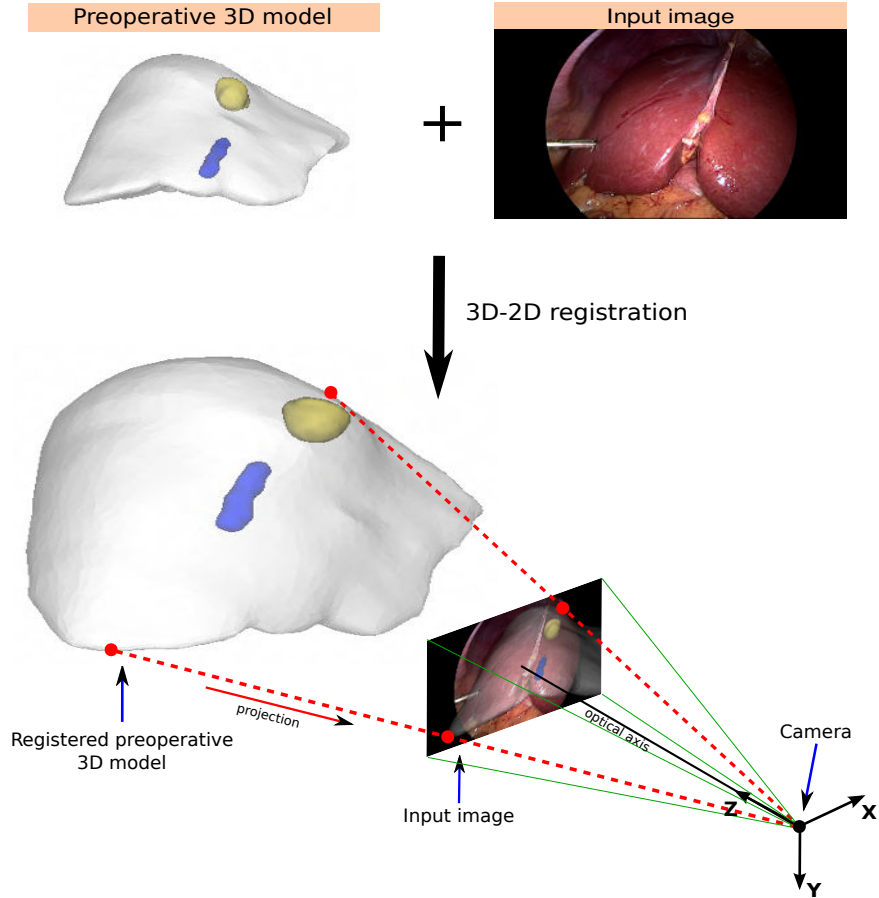


Figure 2: Registration of a preoperative 3D liver model with a laparoscopic image. The preoperative 3D model is extracted from CT and the camera represents the laparoscope. The preoperative 3D model comprises the liver volume whose external surface is in gray and parts of its inner anatomy, namely a subsurface tumour in yellow and vein in blue.

64 surface reconstructed by segmenting the preoperative volume. From these, the state-of-the-
 65 art registration methods are either *manual* [17] or *automatic* [2, 3, 9]. In [17], the preoper-
 66 ative 3D model is rigidly registered to the laparoscopy image by means of user interaction.
 67 In [2, 3, 9], the preoperative model is deformed following a biomechanical model via an It-
 68 erative Closest Point (ICP)-like procedure to fit visual cues extracted from the laparoscopy
 69 image. These visual cues are anatomical landmarks including the falciform ligament and
 70 the inferior ridge, and the silhouette. The current manual and automatic approaches both
 71 present important shortcomings, illustrated in Figure 3. In [17], the rigidity assumption is

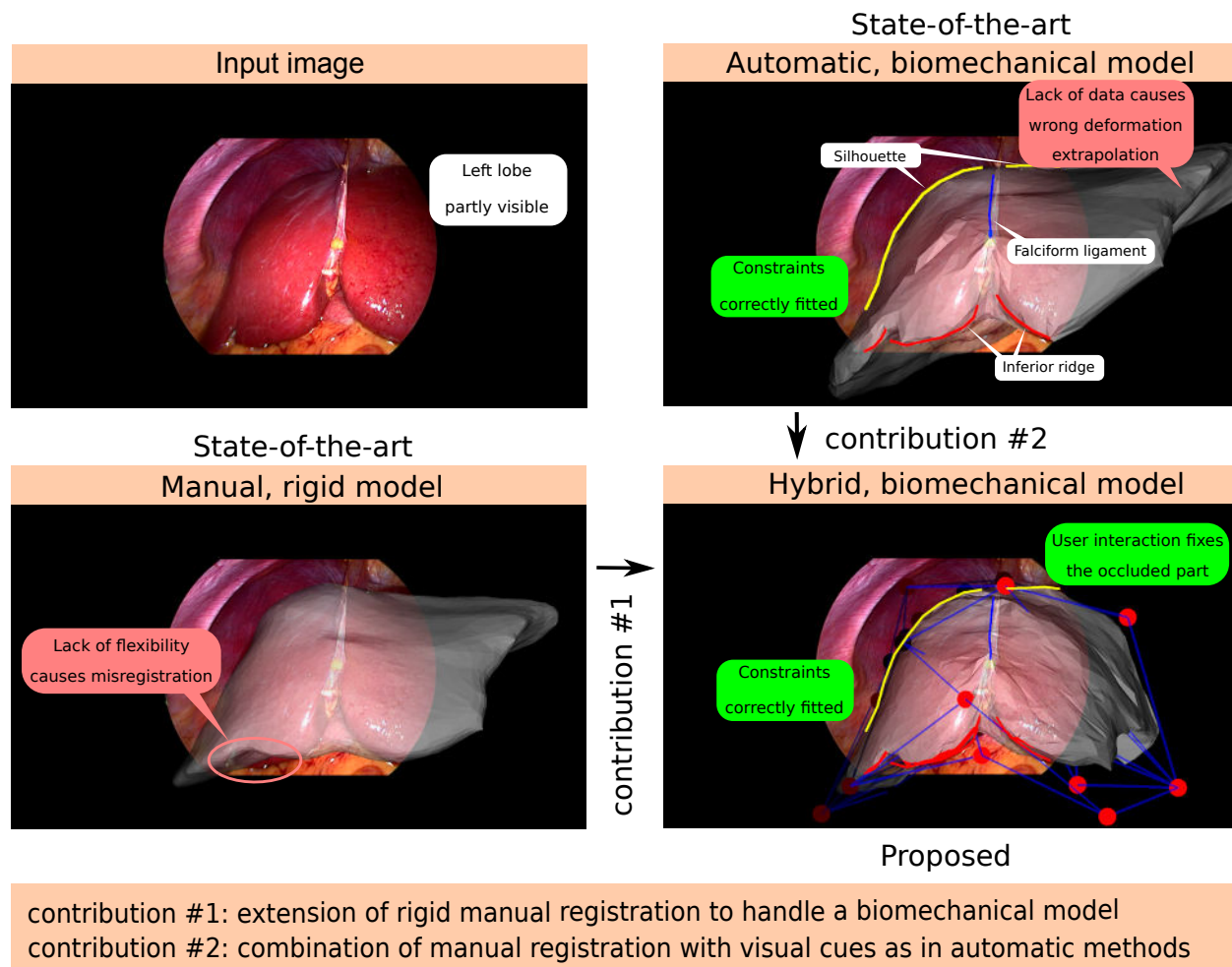


Figure 3: Registration results delivered by the state-of-the-art methods and the proposed one. (top left) The input laparoscopic image. (top right) Results from the automatic method [3] based on visual cues (with liver parenchyma overlaying in gray, and contour constraints in yellow, blue and red). (bottom left) Results of the manual rigid registration method [17]. (bottom right) Results of the proposed hybrid method, combining visual cues with a biomechanical model through cage-based tactile interaction. The cage’s control points (red dots) are used to edit the registration simultaneously with an automatic optimization procedure exploiting the visual cues.

72 far too restrictive to accurately model the liver deformation. In [2, 3, 9], the visual cues
 73 are sparse and do not convey enough information to unambiguously constrain registration.
 74 Though the reasons are different, this results in both cases in misregistration, impairing the

75 reliability of AR.

76 We propose an *hybrid* registration approach. The key idea is that the manual and auto-
77 matic approaches are highly complementary. Our hybrid approach extends and draws on
78 the strengths of both by combining user interaction with visual cues and a biomechanical
79 model. In other words, the rationale is that both the machine and the user perception are
80 valuable and should be taken into account via the visual cues and interaction respectively.
81 In the presence of both user interaction and visual cues, our hybrid approach bundles all
82 constraints in a single registration. In the absence of user interaction, it behaves similarly
83 to the existing automatic approaches. In the absence of visual cues, it allows the user to
84 edit the registration under guidance of the biomechanical model. This is a significant im-
85 provement compared to the existing manual approach as it allows the user to fully express
86 their expertise in anatomy, prior experience and spatial understanding of the case at hand
87 to the system. We have implemented this idea following the cage-based paradigm from the
88 field of shape editing. The cage is a set of handle points enclosing the organ. Dragging these
89 handle points interactively deforms the model. Shape editing is a widely studied problem.
90 The cage-based paradigm is well-adapted to registration owing to its flexibility.

91 Concretely, we implemented our hybrid method with a Qt Graphical User Interface
92 (GUI). Our system is entirely controllable by tactile interaction and may be used in a fast
93 and intuitive manner. We compared our method named *hybrid biomechanical* (HB) quant-
94 itatively in four ways against two previous methods [17], named *manual rigid* (MR) and
95 [3], named *automatic biomechanical* (AB). The first evaluation uses a silicon liver phantom
96 faithfully reproducing the shape of a patient’s liver obtained from CT reconstruction. The
97 phantom was deformed and we used Structure-from-Motion to reconstruct its ground-truth
98 3D shape. The registration was then tested for 20 views from 4 different deformation datasets
99 of 5 views each. The registration error is defined as the average distance between vertices of
100 the preoperative and ground-truth models. The registration error was evaluated for the vis-
101 ible and hidden parts. The second evaluation was performed over 7 images from 7 patients.
102 The registrations were performed for every patient by 5 surgeons. Their manual interactions

103 included the visual cues marking for AB and HB. The obtained registration results were used
104 to evaluate and compare the inter-user registration variability, along with the 2D reprojec-
105 tion errors in the original view used for registration and a control view acquired from the
106 laparoscope inserted in another optical trocar. The registration variability, defined as the
107 root mean square of the standard deviation of the vertex positions, was evaluated over all the
108 vertices and over the visible ones on the registered 3D model. The third evaluation consisted
109 in measuring 2D reprojection errors measured between the set of occluding contour frag-
110 ments of the liver visible in the laparoscopy image and the boundaries of the registered 3D
111 model’s silhouette in both the original and control views. The fourth evaluation consisted
112 in measuring registration errors on an ex-vivo sheep liver. Three inner artificial tumours
113 were injected into the liver. CT scans of the liver’s initial and deformed states were made
114 to obtain the preoperative and groundtruth 3D models respectively. The registration error
115 was evaluated for two laparoscopic views for MR, AB and HB for the three tumours.

116 **1.1 Related Work**

117 We review related work on biomechanical registration of a preoperative 3D liver model with
118 laparoscopic images and on 3D shape editing.

119 **1.1.1 Liver Preoperative Model Registration**

120 This review is split in methods using the image contents only in monocular laparoscopy and
121 methods using other modalities.

122 **Monocular laparoscopy.** Methods [2, 3, 9] process a single laparoscopy image with manu-
123 ally marked contour constraints representing the visual cues. More specifically, [2, 3] rely on
124 contours, namely the falciform ligament and inferior ridge, and the silhouette, whereas [9]
125 relies solely on the silhouette. Method [3] also uses a shading cue while [2] exploits envir-
126 onment priors modeling the effect of the pneumoperitoneum and gravity. Exploiting these
127 environment priors remains difficult in vivo because of the unknown boundary conditions

128 involving the viscera. These methods are highly desirable as being compatible with standard
129 laparoscopy. One of their main limitations is that occluded parts are still poorly registered
130 which has a direct impact on the location of registered tumours and vessels.

131 **Non-monocular laparoscopy.** Methods [10, 11, 12] use a stereo-laparoscope to recon-
132 struct the visible surface of the intraoperative liver shape. In [10], the liver’s 3D contour
133 boundaries are automatically detected on the visible surface and used to constrain regis-
134 tration. Method [11] extracts 3D features on the preoperative and intraoperative surface
135 meshes and robustly finds correspondences using the feature descriptors and locations. The
136 two shapes are then aligned through a rigid registration. Method [12] reconstructs surface
137 patches of the intraoperative liver shape. The stereo-laparoscope is tracked using an optical
138 tracking system. This allows one to localize the patches in world coordinates and use them
139 to constrain registration. Method [13] uses a tracked stylus to let the user enter landmarks
140 on the liver surface. Because the pose of the landmarks is known, they directly serve as
141 registration constraints. Method [18] uses intraoperative CT scans to constrain registra-
142 tion. Finally, method [14] registers an intraoperative CT scan to the laparoscope by imaging
143 the laparoscope’s distal end itself within the CT volume and combining this with shading.
144 These methods share a dependency on non standard laparoscopy or special hardware to
145 solve registration. Nonetheless, with the exception of [18], they do not address the problem
146 of registering the liver’s hidden parts, strongly limiting their usage for AR.

147 **1.1.2 Interactive Shape Editing**

148 Shape editing refers to the change of a model’s surface through a set of handles either
149 part of or connected to it. Existing approaches can be divided in four main categories,
150 depending on how such handles are distributed: point-based [5], curve-based [6], surface-
151 based [7] and cage-based deformations [8]. In a point-based approach, the user provides a
152 set of point displacements, each comprising a point along with its intended motion and region
153 of influence. The way points are distributed does not depend on the shape of the model,

154 but more on the user’s preference. When these points are moved, the object is then warped
155 to match the displacement constraints [5]. In curve-based approaches, the deformations are
156 controlled by one or more curves. The control points are distributed to form a line that the
157 user curves. The deforming object is distorted to map from the source to the destination
158 curves [6]. The surface-based approaches consist in deforming the object when a surface
159 patch is modified by translating a set of control points. The control points are directly
160 located on the surface of the model. One of the main difficulties is to find a way to attach
161 sample points on the object to the deforming patch [7]. The cage-based approaches use a
162 cage that encloses the object. This cage can have a fixed shape such as a cuboid [8], or
163 can be adapted to the shape of the object to be deformed [15]. The shape of this cage is
164 altered by repositioning control points. The resulting cage distortion is then transferred to
165 the object.

166 **2 Materials and Methods**

167 **2.1 Hybrid Registration**

168 We first describe the principle and pipeline of our method. We then describe our implement-
169 ation of the biomechanical model and the visual cues constraints. We finally show how these
170 integrate with cage-based user interaction.

171 **2.1.1 Principle and Pipeline**

172 Our hybrid registration method takes as input a preoperative 3D model and a single lap-
173 aroscopic image. Its principle is to combine a biomechanical model and the manual and
174 automatic registration approaches. These respectively use user interaction and visual cues
175 extracted from the image to solve for registration. Our method thus rests on three sets of
176 constraints. The first two are borrowed from [3]. These are a biomechanical model based on
177 the Neo-Hookean elastic model and the use of the falciform ligament and inferior ridge as
178 curve correspondences, and the silhouette. The third set of constraints are the cage-based

179 constraints to model user interactions. Concretely, the preoperative 3D model is represented
180 by a tetrahedral mesh and optimization follows the principle of position-based dynamics [16].

181 The pipeline of our method is illustrated in Figure 4. It has 7 main steps. The first
182 two steps are similar to [3]: in step (1), the user marks the falciform ligament, inferior ridge
183 and silhouette on the laparoscopy image and in step (2), the user marks the corresponding
184 contours on the preoperative 3D model. In step (3), the system generates a cage enclosing
185 the preoperative 3D model, to be used for user interaction at step (6). In step (4), the
186 cage’s control points and the preoperative 3D model are co-tetrahedrised in order to obtain
187 a single tetrahedral model. In step (5), an initial registration is computed using only the
188 visual cues, following an automatic method [3]. This initial registration is required to initiate
189 interactive registration. In step (6), the user interactively edits the registration by moving
190 the cage’s control points. The registration is updated in real-time to provide the user with
191 live feedback. Importantly at this step, both the cage’s control points and the visual cues
192 are used to update the registration. Finally, once the user is satisfied with the registration,
193 step (7) augments the laparoscopic image with hidden anatomical elements transferred from
194 the preoperative 3D model.

195 **2.1.2 Biomechanical Model and Visual Cues Constraints**

196 The biomechanical model is created by augmenting the preoperative 3D model with the
197 isotropic Neo-Hookean elastic model [16]. This non-linear hyperelastic model works well for
198 registration in laparoscopy, which involves moderate deformations, under the following three
199 conditions: after the liver is freed from the falciform and round ligaments (which is always
200 done at the start of surgery for accessibility purposes), when there is no strong external
201 forces from the tools, and before any resection takes place. The associated mechanical
202 parameters are set to generic values measured for the liver, namely the Young’s modulus
203 to $E = 60,000Pa$ and Poisson’s ratio to $\nu = 0.49$ [2]. The contour constraints rely on
204 anatomical landmarks which are the ridge, the falciform ligament, and the silhouette contours
205 to constrain the deformation. The ridge contour is located at the bottom of the liver, it is

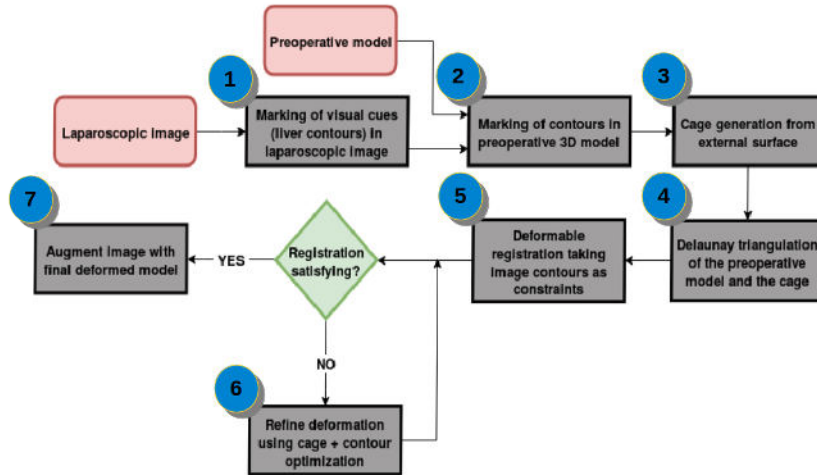
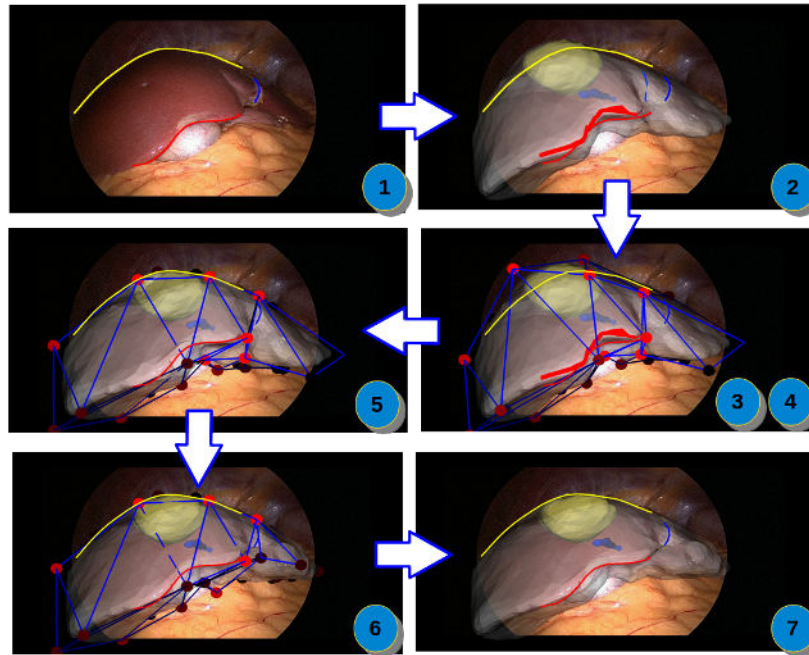


Figure 4: Pipeline of the proposed hybrid 3D to 2D deformable liver registration method. The liver surface mesh is overlaid in gray, its subsurface tumour in yellow and vein in blue. The contours associated to the silhouette, the falciform ligament and the ridge are marked in yellow, blue and red, respectively. The cage is rendered in blue wireframe and its associated control points with red dots.

206 almost always visible and it has a very distinctive profile. The falciform ligament attaches
 207 the liver to the abdominal wall. It is located in the separation zone between the left and

208 right lobes. It is cut in the early stage of surgery to let the liver move freely. Its location is
209 then made clearly visible on the liver external surface. These two sets of contour fragments
210 are stationary. Their correspondence with vertices in the preoperative 3D model remains
211 fixed for the entire registration procedure. The last set of contour is the liver silhouette,
212 imposing the liver model to not deform beyond those boundaries. Unlike for the ridge and
213 the falciform ligament contours, the silhouette contours are not stationary and the associated
214 set of constraints must be updated during the registration procedure. Because a silhouette
215 contour corresponds to the upper convex diaphragmatic surface of the liver, which is a very
216 smooth region, the silhouette curve can slide on the surface as the optimization progresses. In
217 contrast, because of the very well defined curvature profile of the ridge, and the narrowness
218 of the falciform ligament landmark, we can make use of the same set of vertices in the
219 3D preoperative model as correspondences for their 2D counterparts, and thus prevent the
220 model to freely ‘slide’ on the surface during optimisation. All these contour constraints
221 are introduced in the optimization algorithm using an ICP technique. We do not explicitly
222 model physical factors like diaphragm pressure, pneumoperitoneum or pre-stretching of the
223 liver as boundary constraints for the registration process, as these are not measurable, both
224 preoperatively and intraoperatively. Instead, these effects are handled by the interactions of
225 the surgeon with the preoperative 3D models through the surrounding cage.

226 **2.1.3 Cage-based User Interaction**

227 An intuitive and easy-to-use interface allowing the user to edit the liver’s shape in a way
228 that respects its properties and the visual constraints must be proposed. This is achieved
229 through the use of a cage. This has a good trade-off between editing flexibility, namely
230 the possibility to edit at an appropriate spatial frequency, and user friendliness. The cage
231 is represented by a mesh composed of a very limited number of control points. These are
232 obtained following the cage initialization procedure defined in [15] so that the cage encloses
233 the input preoperative 3D model. Once the cage is generated, it is linked to the preoperative
234 3D model through a Delaunay tetrahedralization applied on all the vertices, namely the cage,

235 the liver and its inner structures vertices. During the registration, they are all optimized
236 using the same material model. An example of a generated cage is shown in Figure 3.

237 Making the constraints derived from the cage movable during the optimization proced-
238 ure is not trivial. We propose to embed once and for all the cage’s control points into the
239 volumetric model of tetrahedral topology built from the preoperative 3D liver model. An-
240 other possible solution would consist in creating a cage according to the model deformation
241 at every iteration, which would however significantly harm the software usability. When a
242 cage’s control point is moved during the optimization, all the vertices belonging to the liver
243 model adjacent to it are moved accordingly. This allows the user to handle a set of vertices
244 simultaneously over a model region. These deformations are compensated by the constraints
245 described in section 2.1.2 at the same time. During optimization, a single iteration of the
246 contour-based optimization is run for every change in position of the cage vertices in order
247 to increase the responsiveness of the deformation.

248 **2.2 Tactile Graphical User Interface**

249 The proposed GUI is shown in Figure 5. It is divided in four sections. First, the visualization
250 area in which the laparoscopic image and the preoperative 3D model are shown. The user
251 can position the preoperative 3D model and mark the contours using tactile gestures or the
252 keyboard and mouse. Second, the left toolbar, which is used to either import or export the
253 laparoscopic image and the preoperative 3D model. Third, the right toolbar, which is used
254 to modify the appearance of the preoperative 3D model, to mark the visual cues and to
255 launch registration. Fourth, the bottom toolbar, which controls the size of the visualization
256 area, lets the user activate the cage-based editing mode, and implements miscellaneous other
257 functionalities.

258 Registration begins with a user click on  to set the laparoscope parameters obtained
259 from a prior calibration procedure. The button  is then used to load the laparoscopic image
260 and the button  to load the preoperative 3D model. The visual cues are marked both in
261 the laparoscopic image and the preoperative 3D model with the help of the controls located

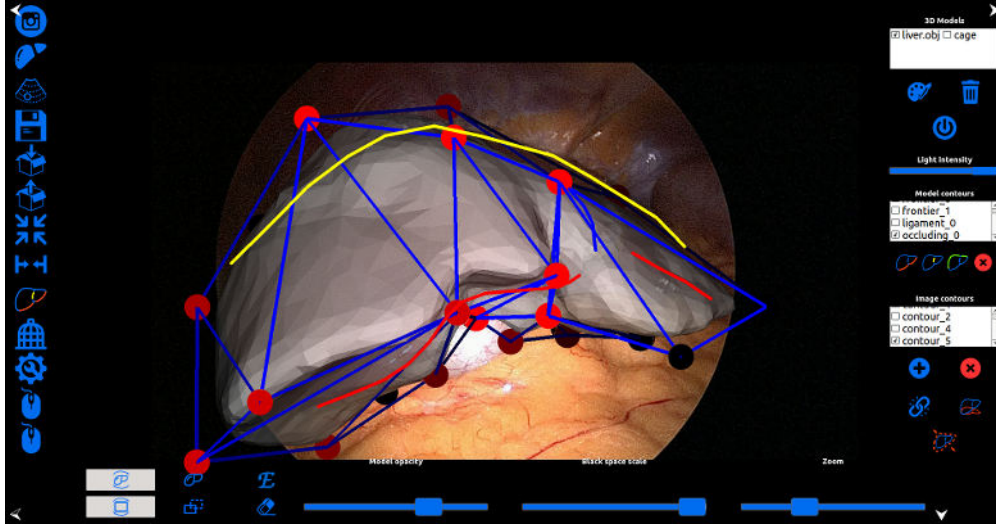


Figure 5: Proposed tactile Graphical User Interface for our hybrid method.

262 in the right toolbar. A rigid registration is done automatically so that the preoperative
 263 model fits the liver approximately in the laparoscopic image. The nested cage is generated
 264 by clicking on . The user then proceeds to match the contours by clicking on . The
 265 preoperative 3D model can then be translated and rotated so that they approximately fit
 266 the image. Automatic contour-based deformation is then launched by clicking on . Once
 267 it completes, the user can proceed to edit the registration using the cage by clicking on the
 268 button . The vertices of the cage may be dragged while the system displays the registration
 269 combining the visual cues and the cage in real-time.

270 Our AR software is setup on a PC computer running Linux. In the OR, this computer is
 271 connected via a capture card to the laparoscopy column in order to capture the laparoscopic
 272 video stream. The computer is located close to the other screens so that the surgeon has a
 273 direct view of the augmentation (see Figure 6). It is equipped with a tactile screen, which
 274 can be directly used by the surgeon.



Figure 6: Usage of our AR guidance system (left computer) in the operating room to perform a laparoscopic tumour resection.

275 **3 Results**

276 This section is divided in three parts. In the first part, results of an accuracy evaluation
277 of the registration on a liver phantom are reported. In the second part, the registration
278 variability and the reprojection errors in control views are evaluated on in-vivo liver data
279 from the hepatobiliary and pancreatic surgery department of the CHU Estaing hospital in
280 Clermont-Ferrand, France. In the third part, the registration accuracy is evaluated with
281 respect to inner artificial tumours injected into an ex-vivo sheep liver. We compared our
282 method HB quantitatively in two ways against two previous methods, MR [17] and AB [3].

283 We recall that for pathologies such as colorectal cancer liver metastasis (CRLM) and
284 hepatocellular carcinoma (HCC), a resection margin of 1 cm should be considered if possible
285 [20, 21]. Thus, we consider a registration error nearby the tumour of a centimeter or lower
286 as successful.

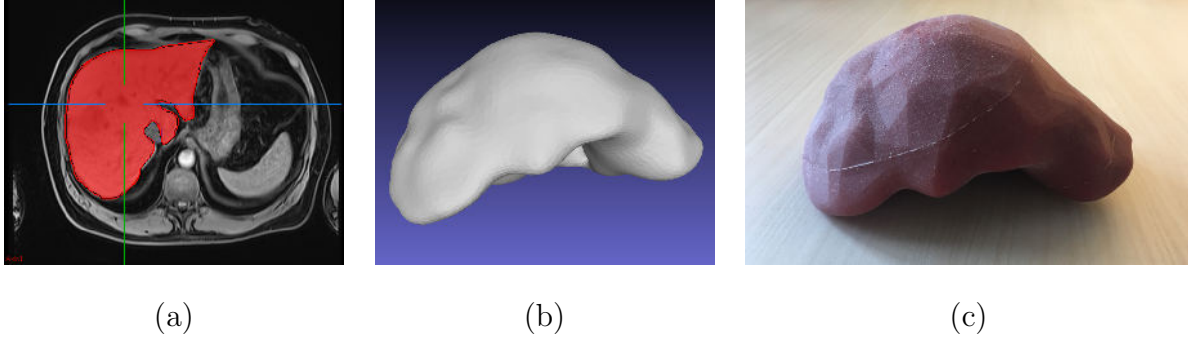


Figure 7: (a) Segmentation of the liver in a patient CT image. (b) Preoperative 3D liver model obtained from the segmentation and used to 3D print a model for (c) the liver phantom used for the proposed accuracy evaluation of the registration methods.

287 3.1 Accuracy Evaluation on a Liver Phantom

288 The accuracy of the proposed registration method is evaluated using a 3D printed liver
 289 phantom made of silicon (Figure 7(a)) aiming to simulate the bio-mechanical properties of a
 290 real liver. The liver phantom was built as follows. The preoperative 3D model was segmented
 291 from CT data of a real patient. A mold of this 3D liver was generated and 3D-printed. The
 292 mold was finally filled with silicon (Figure 7). We used an Ecoflex 00-20 silicon material
 293 made by Smooth-On Inc. which has a Young elastic modulus of 60kPa [22], very close to
 294 the 50 - 60kPa of a human liver.

295 The principle of this experiment is as follows. The liver phantom is deformed and its
 296 shape reconstructed using the Structure-from-Motion software Agisoft Photoscan [19], as
 297 shown in Figure 9. Then, we take N views out of those used to reconstruct the phantom's
 298 shape as input images for the registration procedure. The CAD model from which the
 299 phantom has been printed is used as the input preoperative 3D model and is registered
 300 following the proposed registration method (Figure 8).

301 This experiment is performed for $M = 4$ phantom deformations, shown in Figure 9, and
 302 $N = 5$ different views per deformation. The registration error, defined as the average distance
 303 between vertices of the registered preoperative and ground-truth models, is reported in Table
 304 1. As we compared the distances between all the vertices and not only the ones involved

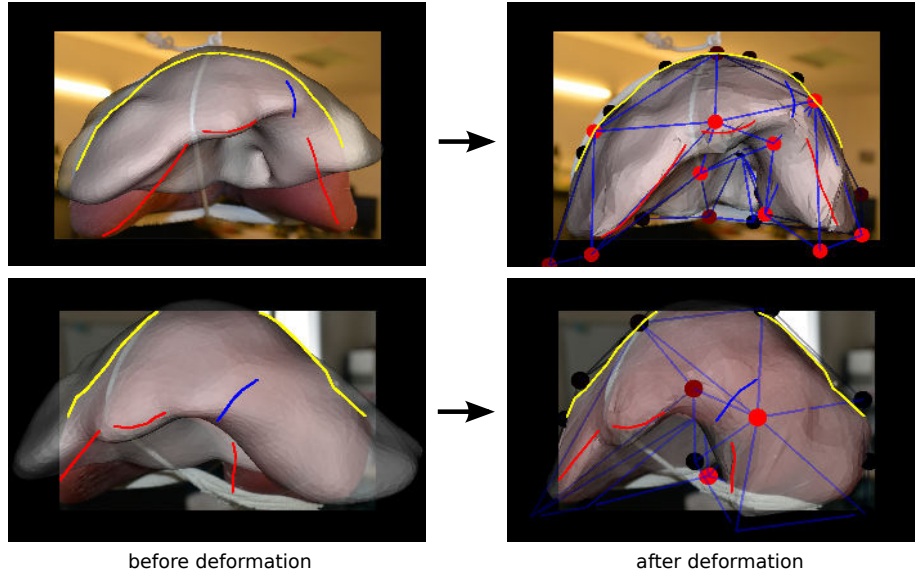


Figure 8: Registration of preoperative 3D model on phantom data with HB method.

305 in the registration, it can be considered a measurement of a target registration error (TRE)
 306 [23]. We report the errors for two sets of vertices: those associated to the entire registered
 307 model and those restricted to its visible part, namely the anterior part, corresponding to a
 308 usual laparoscopy image.

309 HB shows the lowest registration error. The error of MR is noticeably higher as the
 310 method does not deal with the phantom deformations. The registration error of AB is overall
 311 lower than MR's. It shows that the visual cues in AB well constrain the biomechanical model.
 312 HB shows lower errors than AB as misaligned parts can be corrected while preserving the
 313 visual cues and biomechanical constraints. The standard deviations are the lowest for HB
 314 which shows that the method also provides the most stable results. In some cases, such as
 315 for example the registrations AB performed on dataset 1 or HB on dataset 4, the average
 316 error over the entire liver is lower than the error over its visible part, which reveals lower
 317 registration errors on hidden parts. To better illustrate this, error distributions over the
 318 entire liver's vertices are shown in Figure 10.

319 The registration accuracy is also evaluated with varying visibility of the liver phantom.
 320 A decreasing Field of View (FoV) was simulated by adding a circular black border to the

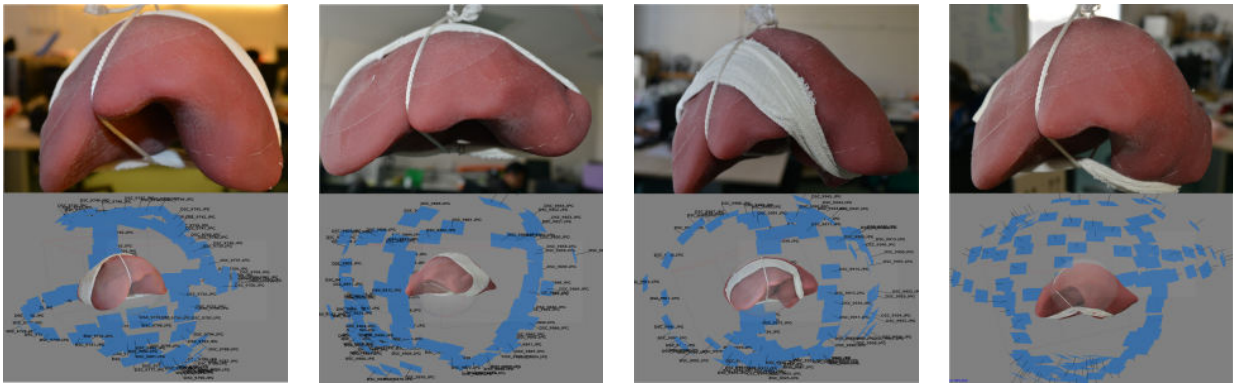


Figure 9: The deformations applied to the 3D printed phantom used in our first set of experiments. Top: deformed phantom. Bottom: 3D model, reconstructed with the Agisoft Photoscan software, used as ground-truth in our experiments.

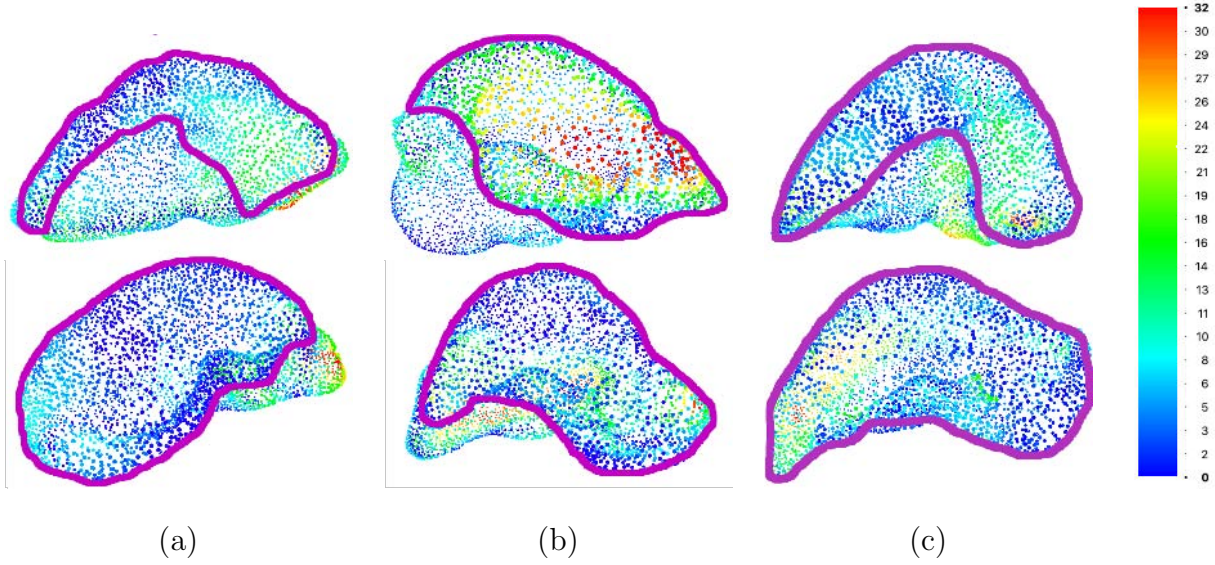


Figure 10: Error distribution over the registered phantom models using (a) MR, (b) AB and (c) HB. The colors range from blue which corresponds to the lowest registration errors to red which corresponds to the highest ones. Distances are in millimeters. The visible parts correspond to the areas limited by the purple curve. Top: cases associated to a registration error higher on the visible parts than on the hidden parts. Bottom: cases associated to a registration error higher on the hidden parts than on the visible parts.

Registration error for whole liver (mm)			
Dataset ↓	MR	AB	HB
1	09.00 ± 2.82	<u>05.35 ± 1.26</u>	04.10 ± 0.39
2	<u>06.19 ± 2.26</u>	08.65 ± 5.04	05.05 ± 0.9
3	12.23 ± 1.84	<u>10.32 ± 2.17</u>	08.46 ± 1.26
4	08.60 ± 1.9	<u>06.78 ± 0.8</u>	05.70 ± 0.42
Average	09.01 ± 2.2	<u>07.75 ± 2.31</u>	05.82 ± 0.74
Registration error for visible part (mm)			
Dataset ↓	MR	AB	HB
1	11.09 ± 4.66	<u>07.96 ± 5.3</u>	04.62 ± 1.02
2	<u>06.77 ± 4.43</u>	07.78 ± 4.9	04.11 ± 1.36
3	12.67 ± 5.26	<u>09.43 ± 3.32</u>	05.60 ± 1.66
4	10.46 ± 7.47	06.67 ± 1.03	<u>07.80 ± 1.63</u>
Average	10.24 ± 5.45	<u>07.96 ± 3.63</u>	05.53 ± 1.41

Table 1: Registration errors with respect to ground truth for the phantom experiment. The errors are expressed in millimetres and correspond to the average distance between the registered model’s vertices. Best results are in bold, second best are underlined.

321 images. The registration were performed for a FoV of 100%, 70% and 50%. One image per
322 dataset were used to perform MR, AB and HB registrations. The results are reported in
323 Table 2. Some registration results are illustrated in Figure 11.

FoV →	100%	70%	50%	Avg
MR	07.68	12.47	15.51	11.89
AB	<u>06.75</u>	<u>07.15</u>	<u>07.59</u>	<u>07.16</u>
HB	05.88	06.47	06.60	06.32

Table 2: Registration errors (in mm) for decreasing FoV using MR, AB and HB methods. The best results are in bold and the second best underlined.

324 The registration accuracy is also assessed for AB with a varying number of tetrahedrons

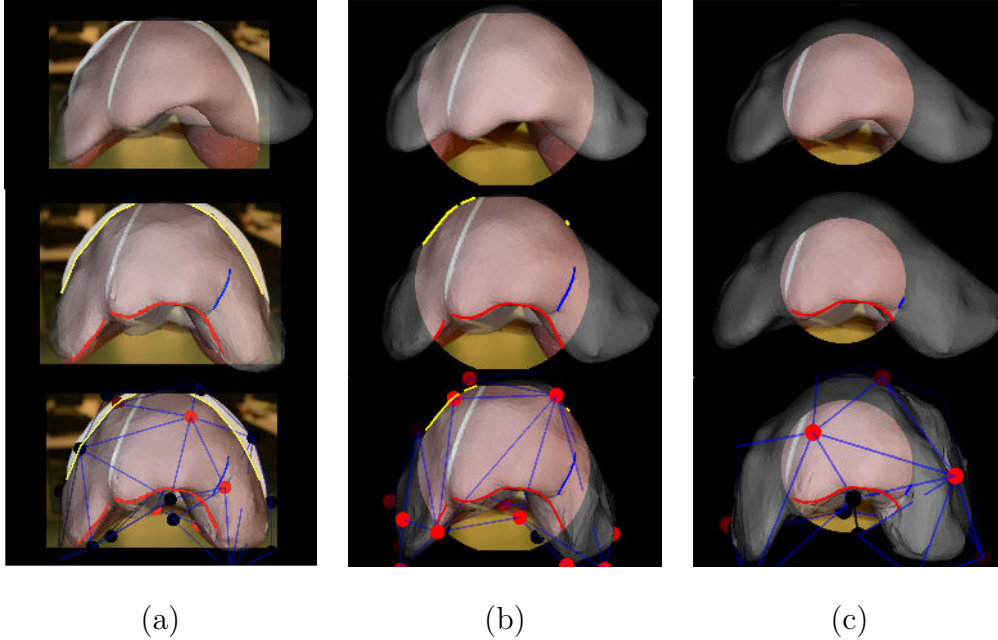


Figure 11: Registration results for 3 different FoV on the first dataset: a FoV of (a) 100%, (b) 70% and (c) 50%. The top images correspond to registrations using MR, the middle images to registrations using AB, and the bottom images to registrations using HB. The circles represent the FoV applied in each case.

325 composing the biomechanical model. Three preoperative 3D models were created, com-
 326 prising tetrahedrons obtained by the triangulation applied on 8000, 4000 and 2000 vertices
 327 respectively. AB was run on one image per dataset. The registration error is reported in
 328 Table 3.

Dataset →	1	2	3	4	Avg
2000 vertices	<u>06.22</u>	05.46	07.43	07.62	06.68
4000 vertices	04.28	03.88	<u>11.46</u>	<u>07.39</u>	<u>06.75</u>
8000 vertices	07.06	<u>04.59</u>	11.55	06.71	07.47

Table 3: Registration errors for the AB method using preoperative 3D models with varying number of vertices. The errors are expressed in millimetres and correspond to the average distance between the registered model’s vertices.

3.2 Variability and Control View on in vivo Liver Data

A high variability of the registration results obtained from different operators is a sign of unreliability of the registration solutions. High reprojection errors in control views reveal a bad registration. We propose to assess both registration variability and reprojection errors in control views on real patient’s data (Figure 12).

3.2.1 Variability for MR, AB and HB registrations

We asked 5 surgeons to perform MR, AB and HB registrations on 7 different patient datasets. Before performing registration, the surgeons were also provided with short videos acquired during the surgery’s exploratory stage. The laparoscope was inserted in different trocars to let the surgeons have a wider scene perception. Table 4 reports the average of the vertex-to-vertex root-mean-square deviation (RMSD) over the surgeons for MR, AB, and HB registrations. For a patient, the RMSD measures how different the registered shapes are between surgeons. It differs from the standard deviations reported in Table 1 which correspond to the deviations of the registration errors computed from ground truths.

Model	Method ↓ Patient →	1	2	3	4	5	6	7	Avg
Whole liver	MR	06.50	14.42	<u>17.33</u>	10.38	09.89	<u>11.93</u>	11.53	11.71
	AB	07.51	20.93	33.78	14.89	<u>12.99</u>	10.51	13.97	16.37
	HB	<u>06.82</u>	<u>19.39</u>	16.45	<u>13.29</u>	13.23	17.37	<u>12.46</u>	<u>14.14</u>
Visible	MR	<u>04.88</u>	12.16	<u>09.61</u>	<u>09.57</u>	07.98	<u>09.99</u>	05.28	08.49
	AB	06.56	18.83	30.57	09.63	<u>08.79</u>	08.80	<u>10.96</u>	13.45
	HB	04.80	<u>17.76</u>	09.05	06.96	09.58	14.32	11.59	<u>10.58</u>
Tumour	MR	06.07	12.09	<u>08.71</u>	09.52	07.05	<u>14.86</u>	05.26	09.08
	AB	07.41	18.33	29.87	11.60	<u>07.52</u>	10.29	<u>07.08</u>	13.16
	HB	<u>06.59</u>	<u>17.60</u>	07.69	<u>10.79</u>	11.05	16.83	07.21	<u>11.11</u>

Table 4: Registration variability (in mm) over the surgeons on 7 in vivo datasets.

The average variability for all the patients is of 9.1 mm for MR, 13.2 mm for AB, and 11.1 mm for HB. One of the key results is that, while HB offers a higher flexibility on the

345 model deformation than for AB, the overall registration variability remains lower. MR shows
 346 the lowest variability because it has very little flexibility.

347 3.2.2 Control View

348 From the registrations made by the surgeons on the in-vivo data, we selected 6 patients for
 349 which we had views of the liver acquired from a different optical trocar. We measured the 2D
 350 reprojection errors as the distance from occluding contours manually extracted from the lap-
 351 aroscopic images to the boundaries of the registered model’s reprojections. It was performed
 352 for both the reference and additional views. Tables 5 and 6 report the 2D reprojection errors
 353 in pixels for the reference and the additional views respectively. Table 7 reports the average
 354 of the reprojection errors for both views.

Patient →	1	2	3	4	5	6	Avg
MR	32.22	34.12	34.68	30.04	18.63	37.99	31.28
AB	15.16	<u>25.67</u>	<u>22.99</u>	<u>15.19</u>	09.20	<u>09.47</u>	<u>16.28</u>
HB	<u>17.23</u>	20.35	13.20	14.97	<u>09.83</u>	08.40	14.00

Table 5: Reprojection error (in pixels) of the in-vivo patient data in the reference view.

Patient →	1	2	3	4	5	6	Avg
MR	<u>33.09</u>	31.69	<u>53.01</u>	37.35	17.40	44.87	36.24
AB	24.07	26.07	58.40	42.78	<u>17.13</u>	<u>26.71</u>	<u>32.53</u>
HB	34.75	<u>28.29</u>	42.19	<u>37.57</u>	15.58	21.95	30.05

Table 6: Reprojection error (in pixels) of the in-vivo patient data in the control view.

Patient →	1	2	3	4	5	6	Avg
MR	32.66	32.90	43.85	33.69	18.02	41.43	33.76
AB	19.62	<u>25.87</u>	<u>40.69</u>	<u>28.98</u>	<u>13.17</u>	<u>18.09</u>	<u>24.40</u>
HB	<u>25.99</u>	24.32	27.69	26.27	12.70	15.17	22.02

Table 7: Reprojection error average (in pixels) of the in-vivo patient data from both reference and control views.

355 The average reprojection errors are much higher for MR than for AB and HB, while HB
356 has the lowest values. The rigid model in MR cannot be correctly aligned to fit the imaged
357 liver.

358 3.2.3 Registration Time

359 The total setup time is 05:56 (5 minutes and 56 seconds) on average in our experiments.
360 This time can be split between time requiring the surgeon’s attention (understanding the
361 scene, marking the landmarks and performing HB registration), which is 04:05, with standard
362 deviation 00:38, and time not requiring the surgeon attention (for the software to initialize
363 the system and compute AB registration), which is 01:05 on average. It is worth noting
364 that, once the surgeon has understood the scene and made the first registration, subsequent
365 registrations on the same patient will take less time.

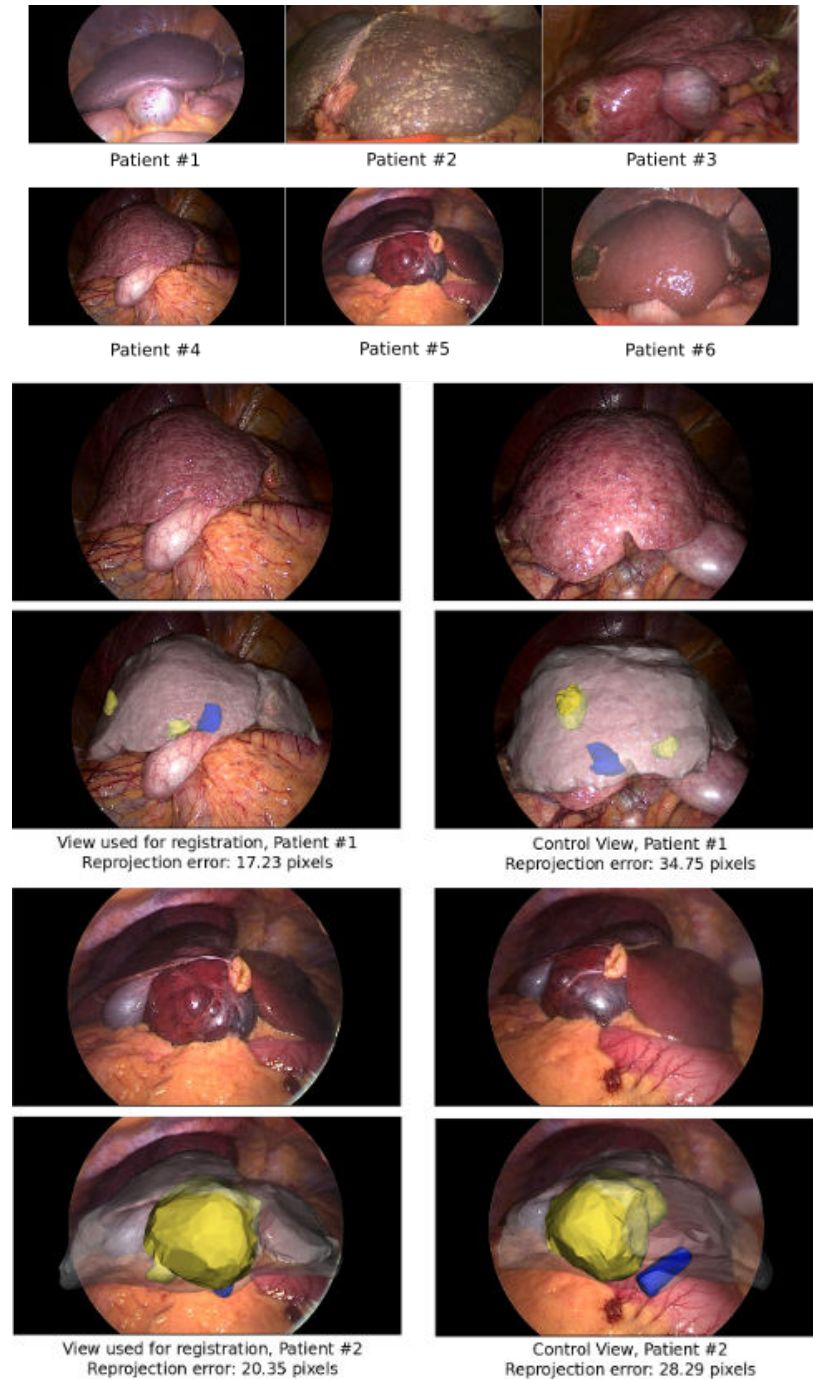


Figure 12: Patient images used for control view evaluation, along with two examples of augmented images and their reprojection errors after HB registration. Laparoscopic images have Full HD resolution (1920 x 1080 pixels). The liver surface mesh is rendered in gray, their subsurface tumours in yellow and veins in blue.

366 3.3 Accuracy Evaluation on Ex-Vivo Sheep Liver

367 We assess the accuracy of our method with respect to inner tumours, by means of an ex-vivo
368 sheep liver which was injected with alginate to create three artificial tumours. Two CT
369 scans of the liver were made. The first one was performed to build the preoperative 3D
370 model to register. The liver was then deformed. The second CT scan was performed on the
371 deformed liver together with a Structure-from-Motion based 3D reconstruction to obtain a
372 registration ground truth (see Figure 13). The registrations were made on two laparoscopic
373 views of the deformed liver using MR, AB and HB for two degrees of visual cues visibility:
374 low and regular. This emulates the possible occlusions from fat and the surrounding organs.
375 The distances between the three registered tumours and their respective ground-truths were
376 then measured. The results are reported in Table 8.

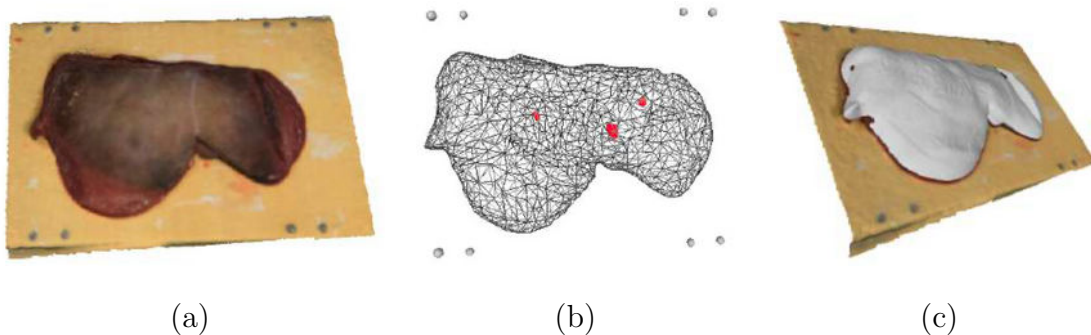


Figure 13: (a) SfM-reconstructed model of the deformed liver. (b) CT-reconstructed models of the deformed liver and tumours. (c) SfM and CT models aligned using ABSOR.

MR method			
Tumour ↓ View →	1	2	Avg
1	02.46	07.02	<u>04.74</u>
2	02.07	03.38	02.72
3	01.57	02.02	<u>01.79</u>

AB method			
Tumour ↓ View →	1	2	Avg
1	02.93	06.65	04.79
2	01.39	02.88	<u>02.13</u>
3	03.79	01.49	02.64

HB method			
Tumour ↓ View →	1	2	Avg
1	01.08	03.65	02.36
2	01.25	02.58	01.91
3	01.19	01.51	01.35

MR method			
Tumour ↓ View →	1	2	Avg
1	00.82	06.56	<u>03.69</u>
2	02.82	02.91	02.86
3	01.50	01.14	<u>01.32</u>

AB method			
Tumour ↓ View →	1	2	Avg
1	01.67	05.78	03.72
2	02.32	02.28	<u>02.30</u>
3	01.36	01.86	01.61

HB method			
Tumour ↓ View →	1	2	Avg
1	01.02	05.58	03.30
2	01.87	02.35	02.11
3	01.31	01.23	01.27

(a)
(b)

Table 8: Registration errors for three synthetic inner tumours on an ex-vivo sheep liver using (a) low visibility and (b) regular visibility of the visual cues. The errors are in millimeters and correspond to the average of the deviations of the registered model’s vertices. For each tumour, the best result is in bold and the second best is underlined.

377 We observe that method HB outperforms for all three tumours and both visibility levels.
378 Methods MR and AB compete for the second best performance, depending on the tumour,
379 though MR is overall slightly better.

380 4 Discussion

381 The registration errors obtained from our method are very promising. The user can expect
382 a similar or lower range of error nearby the tumour area, an error which is below the 1 cm
383 oncologic margin advised in the literature for tumour resection in laparoscopic hepatectomy.
384 The low variability obtained from our method suggests that surgeons have a similar inter-

385 pretation of the scene and were provided with an appropriate tool to edit the model shape
386 accordingly. The lowest variability shown by MR can be explained by the limited control on
387 the model compared to AB and HB, namely restricted to the model’s rigid pose.

388 The time spent by surgeons to perform registration represents a very small portion of the
389 total surgery time. Nonetheless, automating the detection of the landmarks could drastically
390 decrease the manual interaction required from the surgeon, reducing the total registration
391 time and thus improving usability. The problem of landmark detection in the laparoscopic
392 image could be tackled within the framework of deep neural networks. However, it is a diffi-
393 cult problem which to date remains open. Contrarily to organ detection and segmentation,
394 for which recent techniques show compelling results, landmark detection would require the
395 machine to detect curves (which are more difficult to represent than regions in a deep neural
396 network) and to classify them in a type related to their semantics (lying on or off the liver)
397 and geometric properties (being part of the silhouette, for instance). This problem is still
398 open in the computer vision and medical image processing literature.

399 The amount of visible liver also plays an important role in the registration, as shown
400 in Table 2. The lack of visibility affects greatly MR, while AB and HB have better and
401 consistent errors regardless the FoV size. This indicates that in such cases both AB and HB
402 are able to recover the shape of the hidden parts successfully. In general, we see an increase
403 in the registration error for a higher number of vertices/tetrahedrons in the preoperative
404 3D model, as seen in Table 3. Nevertheless this does not always hold for each individual
405 dataset, which means that factors such as the viewpoint and the liver shape play a more
406 important role in the registration than the number of tetrahedrons in the preoperative 3D
407 model. Preliminary results on the ex-vivo experiments show that our method is able to
408 accurately recover the location of the inner tumours for a varying visibility degree of visual
409 cues, even if they are far from any visual constraint and regardless the viewpoint used for
410 registration, as shown in Table 8. The two levels of visibility bring an interesting observation:
411 the stronger the visibility, the smaller the differences between the methods. Specifically, we
412 observe that HB brings a substantial improvement when visibility decreases. This is a

413 sensible result, because when visibility decreases, the added value of the surgeon expertise
414 expressed by their interactions increases, maintaining the performance, while MR and AB
415 may only worsen.

416 The registration performance remains correlated to the technical difficulties inherent to
417 laparoscopic surgery, such as a reduced field of view and limited viewpoint range, which may
418 substantially vary with patient anatomy. For example, the registration of a laparoscopic
419 image where the liver is entirely visible and whose anatomical landmarks can be accurately
420 localised (such as patient #5 in Table 5) is more accurate than one performed on an image
421 where the liver is a partly visible and whose landmarks localisation is ambiguous (such as
422 patient #3 in Table 5).

423 Our approach works on static laparoscopic images, which represent weak inputs, but non-
424 etheless captures the effects of respiration, diaphragm interactions and pneumoperitoneum
425 via the extracted visual cues. In other words, the visual cues inherently represent these
426 complex constraints, which are not capturable otherwise in the routine surgical context of
427 the problem at hand. The strength of our approach is to complement these visual cues which
428 are also weak constraints, by surgeon interactions. This allows our system to take advantage
429 of the observable landmarks from the input laparoscopic image (via the visual cues) and of
430 the surgeons expertise and understanding of the intraoperative scene (via their interactions).
431 Our results confirm that combining a biomechanical model constrained by visual cues and
432 manual interactions is very fruitful. As future work, the registration software will be modi-
433 fied to let the surgeon choose the number of control points in the generated cage, according
434 to the complexity of the liver’s shape. The influence of using a more advanced biomechanical
435 model on the performance should also be evaluated. Further clinical tests have to be made
436 in order to validate our method, notably regarding the location of inner structures after
437 registration on human cases. If such tests confirm an overall registration error lower than 1
438 cm, then the proposed method will give surgeons a reliable basis to guide resection.

439 **Ethical approval:** All procedures involving human participants were in accordance with
440 the ethical standards of the institutional and/or national research committee and with the

441 1964 Helsinki declaration and its later amendments or comparable ethical standards. This
442 study is also supported by an ethical approval with ID IRB00008526-2019-CE58 issued by
443 CPP Sud-Est VI in Clermont-Ferrand, France.

444 **Informed consent:** Informed consent was obtained from the patients included in the
445 study.

446 Conflict of Interest

447 The authors of this article declare no potential conflicts of interest.

448 References

- 449 1. Lamata, P., Lamata, F., Sojar, V., Makowski, P., Massoptier, L., Casciaro, S., Ali, W.,
450 Studeli, T., Declerck J., Elle, O., Edwin, B. Use of the Resection Map system as guidance
451 during hepatectomy. *Surgical Endoscopy*, 24, 2327-2337, (2010)
- 452 2. Ozgur, E., Koo, B., Le Roy, B., Buc, E., Bartoli, A. Preoperative liver registration
453 for augmented monocular laparoscopy using backward-forward biomechanical simula-
454 tion. *International Journal of Computer Assisted Radiology and Surgery*, 13, 1629-1640,
455 (2018)
- 456 3. Koo, B., Ozgur, E., Le Roy, B., Buc, E., Bartoli, A.: Deformable registration of a
457 preoperative 3D liver volume to a laparoscopy image using contour and shading cues.
458 *MICCAI*, (2017)
- 459 4. Bender, J., Koschier, D., Charrier, P., & Weber, D. Position-based simulation of con-
460 tinuous materials. *Computers & Graphics*, 44, 1-10, (2014)
- 461 5. Bechmann, D. and Gerber, D. 2003. Arbitrary shaped deformations with dogme. *The*
462 *Visual Computer* 19 (May), pp. 175-186, (2003)

- 463 6. Barr, A. H. Global and local deformations of solid primitives. *Computer Graphics (SIG-*
464 *GRAPH)* 18, 3 (July), 2130, (1984)
- 465 7. Feng, J., Shao, J., Jin, X., Peng, Q., and Forrest, R. Multiresolution free-form deforma-
466 tions with subdivision surfaces of arbitrary topology. *The Visual Computer* 22, 1 (Jan.),
467 2842, (2005)
- 468 8. Sederberg, T. W. and Parry, S. R. Free-form deformation of solid geometric models.
469 *Computer Graphics (SIGGRAPH)* 20, 4 (Aug.), 151-160, (1986)
- 470 9. Adagolodjo, Y., Trivisonne, R., Haouchine, N., Cotin, S., Courtecuisse, H.: Silhouette-
471 based pose estimation for deformable organs application to surgical augmented reality.
472 *IROS*, (2017)
- 473 10. Haouchine, N., Roy, F., Untereiner, L., Cotin, S.: Using contours as boundary conditions
474 for elastic registration during minimally invasive hepatic surgery. *IROS*, (2016)
- 475 11. Robu, M.R., Ramalhinho, J., Thompson, S., Gurusamy, K., Davidson, B., Hawkes, D.,
476 Stoyanov, D., Clarkson, M.: Global rigid registration of CT to video in laparoscopic liver
477 surgery. *International Journal of Computer Assisted Radiology and Surgery*, 13, 947956
478 (2018)
- 479 12. Thompson, S., Tetz, J., Song, Y., Johnsen, S., Stoyanov, D., Ourselin, S., Gurusamy, K.,
480 Schneider, C., Davidson, B., Hawkes, D., Clarkson, M.: Accuracy validation of an image
481 guided laparoscopy system for liver resection. *Proceedings of SPIE - The International*
482 *Society for Optical Engineering* 9415(09):1-12, (2015)
- 483 13. Clements, L., Collins, J., Weis, J., Simpson, A., Kingham, T., Jarnagin, W. Miga,
484 M.: Deformation correction for image guided liver surgery: An intraoperative fidelity
485 assessment. *Surgery*, 162(3): 537-547, (2017)
- 486 14. Bernhardt, S., Nicolau, S., Bartoli, A., Agnus, V., Soler, L., Doignon, C.: Using Shading

- 487 to Register an Intraoperative CT Scan to a Laparoscopic Image. Computer-Assisted and
488 Robotic Endoscopy. CARE, (2015)
- 489 15. Sacht, L., Vouga, E., Jacobson, A.: Nested cages. ACM Transactions on Graphics,
490 Volume 34, Issue 6, Article No. 170, (2015)
- 491 16. Bender, J., Koschier, D., Charrier, P., Weber, D.: Position-based Simulation of Con-
492 tinuous Materials. Computer & Graphics, (2014)
- 493 17. Nicolau, S., Soler, L., Mutter, D., Marescaux, J.: Augmented reality in laparoscopic
494 surgical oncology. Surgical Oncology, 20(3):189-201 (2011)
- 495 18. Oktay, O., Zhang, L., Mansi, T., Mounney, P., Mewes, P., Nicolau, S., Soler, L.,
496 Chefd'hotel, C., Biomechanically Driven Registration of Pre- to Intra- Operative 3d
497 Images for Laparoscopic Surgery. MICCAI, (2013)
- 498 19. AgiSoft PhotoScan Professional (Version 1.2.6) (Software). (2016)
- 499 20. Margonis G., Sergentanis T., Ntanasis-Stathopoulos I., Andreatos N., Tzanninis I., Sa-
500 saki K., Psaltopoulou T., Wang J., Buettner S., Papalois A., He J., Wolfgang C., Pawlik
501 T., Weiss M. Impact of Surgical Margin Width on Recurrence and Overall Survival
502 Following R0 Hepatic Resection of Colorectal Metastases: A Systematic Review and
503 Meta-analysis. Annals of Surgery, 267(6):1047-1055, (2018)
- 504 21. Zhong FP., Zhang YJ., Liu Y., Zou SB. Prognostic impact of surgical margin in patients
505 with hepatocellular carcinoma: A meta-analysis. Medicine, 96(37):e8043, (2017)
- 506 22. Adams, F., Qiu, T., Mark, A., Fritz, B., Kramer, L., Schlager, D., Wetterauer, U.,
507 Miernik, A., Fischer, P. Soft 3D-Printed Phantom of the Human Kidney with Collecting
508 System. Annals of Biomedical Engineering, 45, 963972 (2017)
- 509 23. Moghari M., Ma B., Abolmaesumi P. A Theoretical Comparison of Different Target
510 Registration Error Estimators. MICCAI, (2008)